

Design and experimental validation of novel optics-based autofocusing microscope

Chien-Sheng Liu · Pin-Hao Hu · Yang-Cheng Lin

Received: 15 April 2012 / Revised: 20 June 2012 / Published online: 15 September 2012
© Springer-Verlag 2012

Abstract This study designs and characterizes a novel precise optics-based autofocusing microscope with both the large linear autofocusing range and the rapid response. In contrast to conventional optics-based autofocusing microscopes with centroid method, the proposed microscope comprises two optical paths, namely one optical path which provides a short linear autofocusing range but an extremely high focusing accuracy and a second optical path which achieves a long linear autofocusing range but a reduced focusing accuracy. The two optical paths are combined using a self-written autofocus-processing algorithm to realize an autofocusing microscope with a large linear autofocusing range, a rapid response, and a high focusing accuracy. The microscope is characterized numerically using commercial software ZEMAX and is then verified experimentally using a laboratory-built prototype. The experimental results show that compared to conventional optics-based autofocusing microscopes with centroid method and a single optical path, the proposed microscope achieves both a longer autofocusing range and a more rapid response with no reduction in the focusing accuracy. Overall, the results presented in this study show that the

proposed microscope provides an ideal solution for automatic optical inspection and industrial applications.

1 Introduction

Machine vision systems are finding increasing use in the manufacturing and inspection fields due to their reliability, relatively low cost, and high throughput [1]. In implementing such systems, it is frequently necessary to focus a camera so as to obtain sharp images of the object of interest [2–8]. As a result, many autofocusing microscopes have been developed in recent years. Existing autofocusing microscopes can be broadly classified as either image-based or optics-based [9]. In microscopes of the former type, the focus position of the objective lens is adjusted by analyzing the image captured by an optical system [10–12]. Such an approach has a low cost and is therefore widely used for many industrial applications [13–27]. However, analyzing the image is highly complex, and thus the autofocusing procedure is rather time consuming [28]. Furthermore, depth of focus constraints limit the maximum focusing accuracy which can be obtained. Many proposals have been presented for resolving these problems by means of optics-based autofocusing methods [29–43]. However, to the best of the current authors' knowledge, these methods achieve a satisfactory focusing accuracy over only a short linear autofocusing range.

Accordingly, this study develops a novel autofocusing microscope which provides both a large linear autofocusing range and a rapid response. The proposed microscope comprises two optical paths. The first optical path is used to achieve a highly precise focusing accuracy over a short linear autofocusing range, while the second path is used to achieve a less-precise focusing accuracy over a longer

C.-S. Liu (✉)
Department of Mechanical Engineering, National Chung Cheng University, No.168, University Road, Minhsiung Township, Chiayi 62102, Taiwan
e-mail: imecsl@ccu.edu.tw

P.-H. Hu · Y.-C. Lin
Laser Application Technology Center Industrial Technology Research Institute, R208, No. 8, Gongyan Rd., Liujia Shiang, Tainan 734, Taiwan
e-mail: PinHaoHu@itri.org.tw

Y.-C. Lin
e-mail: oeic@itri.org.tw

linear autofocusing range. The two optical paths are combined using a self-written autofocus-processing algorithm to achieve a large linear autofocusing range and a rapid response without any loss in the focusing accuracy. The proposed microscope is characterized numerically and is then verified experimentally using a laboratory-built prototype.

The remaining of this article is organized as follows. Section 2 describes the structure of a conventional optics-based autofocusing microscope with centroid method. Section 3 introduces the proposed optics-based autofocusing microscope and compares its output and motion characteristics with those of the conventional microscope with centroid method. Section 4 discusses the experimental characterization of the proposed autofocusing microscope using a laboratory-built prototype. Finally, Sect. 5 presents some brief concluding remarks.

2 Design of conventional optics-based autofocusing microscope with centroid method

2.1 Conventional autofocusing method with centroid method

Figure 1 presents a schematic illustration of the optical path within a conventional optics-based autofocusing microscope with centroid method. When the laser beam strikes point A on the sample surface (located at the focal

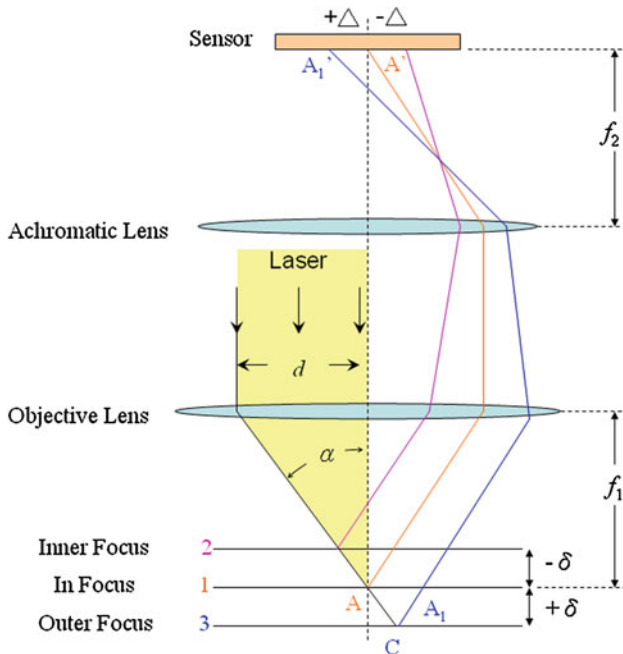


Fig. 1 Schematic illustration of optical path in conventional optics-based autofocusing microscope with centroid method

plane 1 of the objective lens), it is reflected from the surface and is then incident on the CCD sensor at point A'. In accordance with basic geometric principles, the following equation can be obtained:

$$\tan \alpha = d/f_1, \tag{1}$$

where α is the maximum incidence angle of the laser beam, d is the radius of the collimated laser beam, and f_1 is the focal length of the objective lens. When the sample surface is moved from plane 1 to plane 3 (corresponding to a defocus distance of $+\delta$), the laser beam strikes point C on the sample surface and is then reflected. The reflected laser beam intersects plane 1 at point A₁ and is then incident on the CCD sensor at point A₁'. From basic geometric principles, the following equation can be obtained:

$$\overline{AA_1} = 2\delta \tan \alpha. \tag{2}$$

Furthermore, the displacement Δ of the incident point on the CCD sensor can be obtained as

$$\Delta = K\overline{AA_1}, \tag{3}$$

where Δ is the distance between point A' and point A₁', and K is the total magnification of the objective lens and achromatic lens. K can be represented as

$$K = f_2/f_1, \tag{4}$$

where f_2 is the focal length of the achromatic lens. Substituting Eqs. (1), (2), and (4) into Eq. (3), the displacement distance Δ can be obtained as

$$\Delta = \delta \frac{2df_2}{f_1^2}. \tag{5}$$

Equation (5) shows that the displacement Δ and defocus distance δ are linearly related.

Figure 2 illustrates the shape of the laser spot on the CCD sensor given various defocus distances. Note that in the figure, points (X_c, Y_c) and $(x_{centroid}, y_{centroid})$ represent the positions of the geometrical image center and the centroid of the image captured by the CCD sensor, respectively. The image centroid coordinates can be expressed as follows:

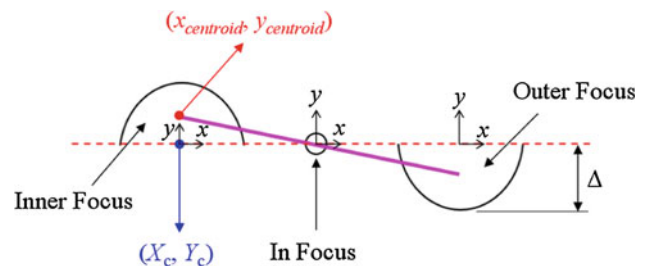


Fig. 2 Schematic representation of laser spot on CCD sensor given different values of the defocus distance

$$x_{\text{centroid}} = \frac{\sum \sum (x - X_c) P_{ij}}{\sum \sum P_{ij}}, \tag{6}$$

$$y_{\text{centroid}} = \frac{\sum \sum (y - Y_c) P_{ij}}{\sum \sum P_{ij}}, \tag{7}$$

where i and j are the row number and column number of the CCD sensor, respectively, and P_{ij} denotes the intensity of the pixel located at the intersection of row i and column j . In the design of the conventional optics-based autofocusing microscope with centroid method, the geometrical image center (X_c, Y_c) is assumed to be located at the origin of the coordinate frame xy and to remain constant. As a result, Eqs. (6) and (7) can be reformulated as follows:

$$x_{\text{centroid}} = \frac{\sum \sum x P_{ij}}{\sum \sum P_{ij}}, \tag{8}$$

$$y_{\text{centroid}} = \frac{\sum \sum y P_{ij}}{\sum \sum P_{ij}}. \tag{9}$$

From Eqs. (5), (8), and (9), it is seen that if the image intensity P_{ij} remains constant over the entire CCD image, a linear relationship exists between the centroid of the image captured by the CCD device and the defocus distance δ . Exploiting this linear relationship, an autofocusing capability can be achieved by driving the objective lens using a position feedback signal derived from the centroid coordinates of the detected image [44].

2.2 Structure of conventional optics-based autofocusing microscope with centroid method

Figure 3 illustrates the basic structure of the conventional autofocusing microscope with centroid method constructed

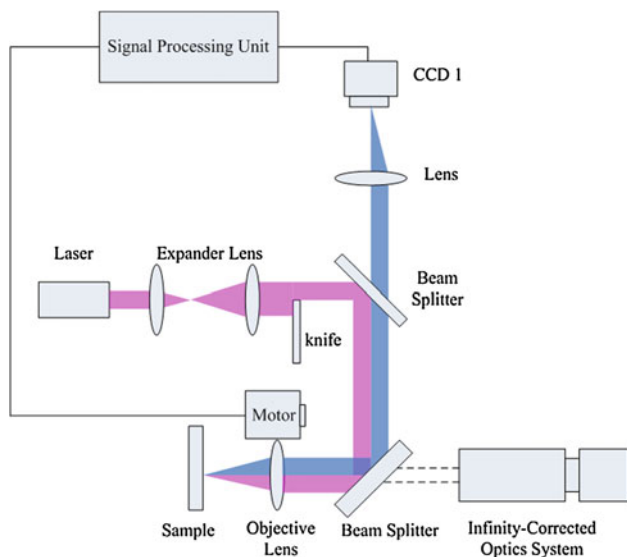


Fig. 3 Structure of conventional optics-based autofocusing microscope with centroid method

for comparison purposes in this study. As shown, the light beam emitted from a laser light source (Hitachi HL6501MG, 658 nm) is expanded and collimated through an expander lens. The collimated laser beam is bisected by a knife (As shown in Figs. 1 and 2, the knife is used to reshape the collimated laser beam into a semicircle beam, so the shape of the laser spot on the CCD sensor varies in accordance with the defocus distance δ .) and is then passed through two beam splitters (BSs). The first BS is designed to achieve an equal reflection and transmission of red light, while the second BS is designed to achieve a high reflection of red light and a high transmission of the remaining visible light (i.e., wavelengths other than 658 nm). The laser beam emerging from the second BS is passed through an objective lens and is incident on the sample surface. Following reflection from the sample surface, the laser beam returns through the objective lens and two BSs, passes through an achromatic lens, and is incident on a CCD sensor (Guppy F-146C, referred to hereafter as CCD1).

In accordance with basic geometric optics principles, the shape of the laser spot (or centroid $(x_{\text{centroid}}, y_{\text{centroid}})$ of the image) on the CCD sensor varies in accordance with the defocus distance δ . In this study, the variation of coordinates $(x_{\text{centroid}}, y_{\text{centroid}})$ was calculated using a self-written autofocus-processing algorithm. An autofocusing capability was then achieved by using a position feedback signal derived from the computed image centroid coordinates to dynamically adjust the position of the objective lens via a linear motor. Real-time images of the sample were captured during the focusing process using an infinity-corrected optical system (Navitar Zoom 6000).

3 Design of proposed optics-based autofocusing microscope

3.1 Structure of proposed optics-based autofocusing microscope

Figure 4 illustrates the structure of the proposed autofocusing microscope. As shown, the light beam emitted from the laser light source (Hitachi HL6501MG, 658 nm) is expanded and collimated by means of an expander lens and is then bisected by a knife. The light beam is then passed through two BSs. As in the conventional autofocusing structure, the first BS is designed to reflect 50 % of the red light and to transmit 50 % of the red light, while the second BS is designed to reflect most of the red light and to transmit the remaining visible light. The light emerging from the second BS is passed through an objective lens and is incident on the sample surface. The laser light reflected from the sample surface passes back through the objective lens and two BSs and is then incident on a third BS, where

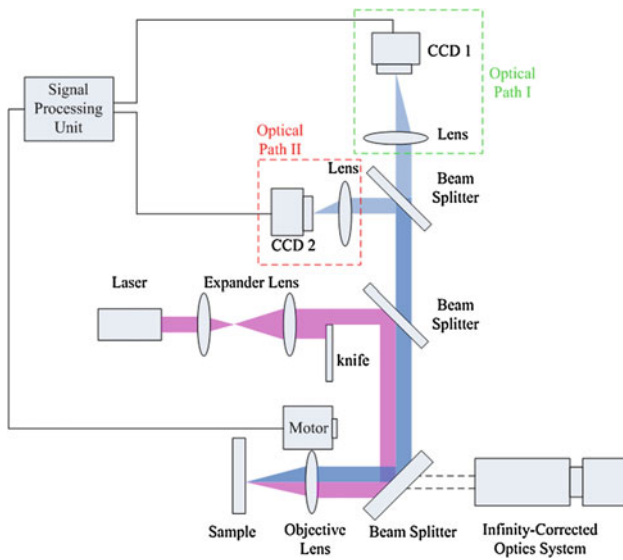


Fig. 4 Structure of proposed optics-based autofocusing microscope

it is split into two separate optical paths. In one optical path (designated as Optical Path I), the light beam emerging from the BS is passed through an achromatic lens and is then incident on CCD1. Meanwhile, in the second optical path (designated as Optical Path II), the light beam passes through another achromatic lens and is then incident on a second CCD sensor (Guppy F-146C, referred to hereafter as CCD2).

From Eqs. (5), (8), and (9), it follows that for a constant displacement Δ of the incident point, the defocus distance δ changes in accordance with changes in the focal length f_2 of the achromatic lens. Therefore, constructing the proposed autofocusing microscope, CCD1 and CCD2 are identical components, but the focal lengths of the achromatic lenses in Optical Paths I and II, respectively, are different. Specifically, the focal length of the achromatic lens in Optical Path I is greater than that of the achromatic lens in Optical Path II, i.e.,

$$\Delta = \delta_1 \frac{2df_{2I}}{f_1^2}, \tag{10I}$$

$$\Delta = \delta_{II} \frac{2df_{2II}}{f_1^2}, \tag{10II}$$

$$f_{2I} > f_{2II}, \tag{11}$$

$$K_I = f_{2I}/f_1, \tag{12I}$$

$$K_{II} = f_{2II}/f_1. \tag{12II}$$

Note that Eqs. (10I) and (10II) refer to Optical Path I and Optical Path II, respectively, and f_{2I} and f_{2II} are the focal lengths of the achromatic lenses in Optical Path I and Optical Path II, respectively. Optical Path I results in a greater total magnification K_I , and therefore provides the

means to accomplish autofocusing over a short linear range but with a high focusing accuracy. By contrast, Optical Path II yields a lower total magnification K_{II} , and therefore provides the means to accomplish autofocusing over a longer linear range but with a lower focusing accuracy. Comparing Figs. 3 and 4, it can be seen that the proposed autofocusing microscope reduces to the conventional optics-based microscope with centroid method if Optical Path II is not activated. However, in implementing the proposed microscope, Optical Paths I and II are both activated and are combined via a self-written autofocus-processing algorithm to achieve autofocusing over a long linear distance with a short response time and with no loss in focusing accuracy.

3.2 Output and motion characteristics of conventional autofocusing microscope with centroid method and proposed autofocusing microscope

Figure 5a illustrates the basic output characteristics of the conventional autofocusing microscope with centroid method (please refer to user’s manual of ATF4 auto focus and scanning sensor, WDI Wise Device Inc.) shown in Fig. 3. As shown, a linear autofocusing range exists within which the centroid coordinates of the image captured by the CCD sensor vary linearly with the defocus distance δ . Within this linear range, the position of the objective lens can be easily adjusted so as to achieve a precise focusing effect by means of a linear motor driven by a feedback signal derived dynamically in accordance with changes in the centroid coordinates. However, as shown in Fig. 5b, if the initial defocus distance δ_1 is located outside of this linear range, the autofocusing procedure should commence by shifting the objective lens through a distance L , where L is equivalent to half the linear range. If the resulting defocus distance δ_2 is still located outside the linear range, the objective lens should be shifted through a further displacement L . This procedure is repeated until the defocus distance (e.g., δ_3) falls within the linear range, at which point the objective lens can be moved directly to the point of maximum focus. Figure 6 presents a flow chart showing the basic steps in the conventional autofocusing procedure with centroid method. From Figs. 5 and 6, it is seen that the objective lens must be shifted multiple times if the initial defocus distance is located far from the linear autofocusing range. Thus, while the structure shown in Fig. 3 enables the point of maximum focus to be reliably determined, the response time may be too long for many applications (e.g., TFT array laser repair and LED substrate laser scribing).

Figure 7 illustrates the output and motion characteristics of the proposed autofocusing microscope. As shown, both optical paths yield a linear autofocusing range. As $f_{2I} > f_{2II}$ (i.e., $K_{2I} > K_{2II}$), the linear range associated with Optical

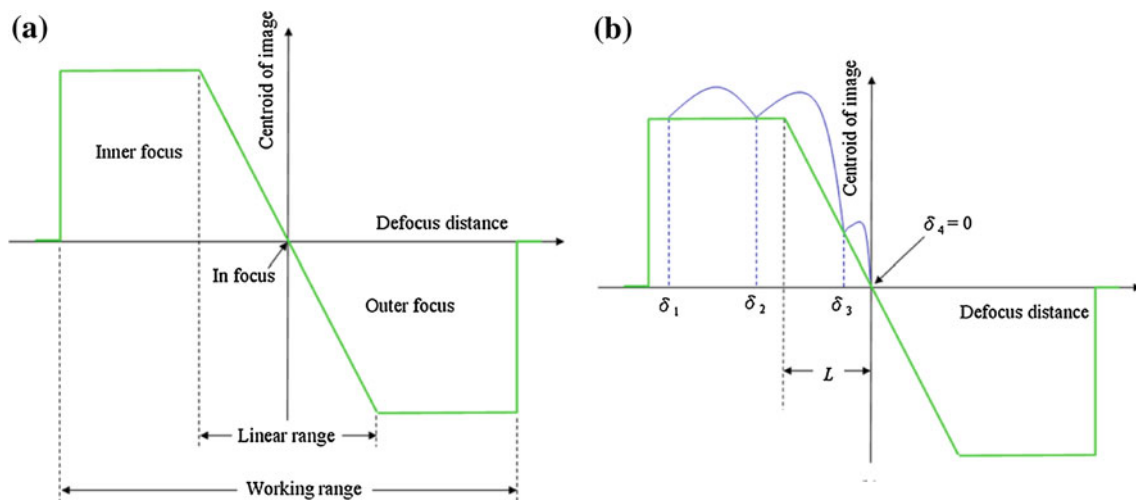
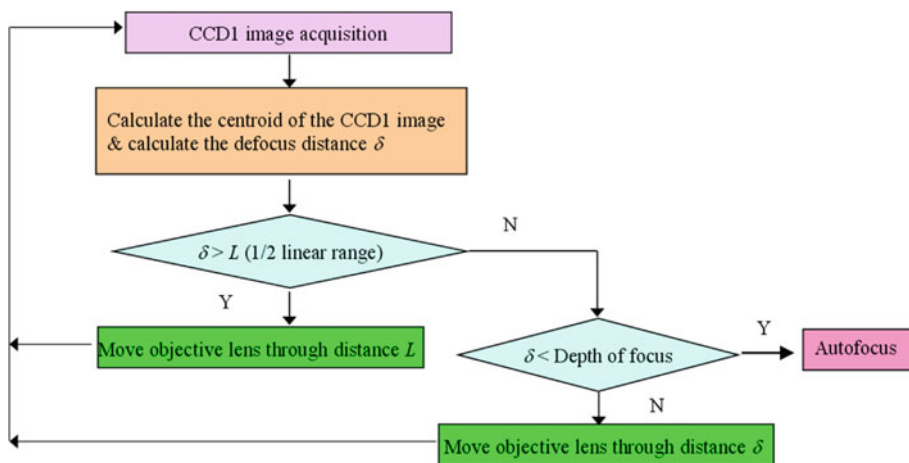


Fig. 5 a Output characteristics and b motion characteristics of conventional autofocusing microscope with centroid method

Fig. 6 Flow chart of autofocus-processing algorithm for conventional optics-based autofocusing microscope with centroid method



Path II is greater than that associated with Optical Path I. If the initial defocus distance δ_1 is located outside of the linear range of Optical Path I, but within that of Optical Path II, the objective lens is shifted through a distance equal to the defocus distance via a linear motor in accordance with the calculated centroid coordinates ($x_{centroid}$, $y_{centroid}$) of the image detected by CCD2 in Optical Path II. However, Optical path II has a low focus accuracy. Therefore, the position of the objective lens is moved to δ_2 , outside of the depth of focus of this system. However, if δ_2 is located within half the linear range of Optical Path I, the objective lens is moved directly to the point of maximum focus. Figure 8 presents a flow chart showing the basic steps in the proposed autofocusing procedure. From Figs. 7 and 8, it can be seen that irrespective of the initial defocus distance δ , the objective lens need be shifted no more than twice in arriving at the point of maximum focus. In other

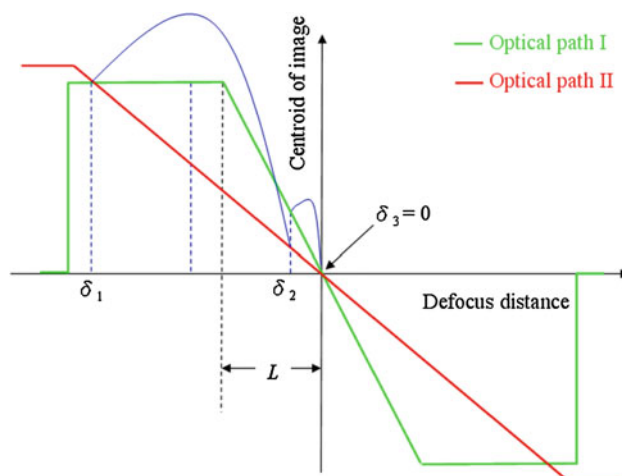
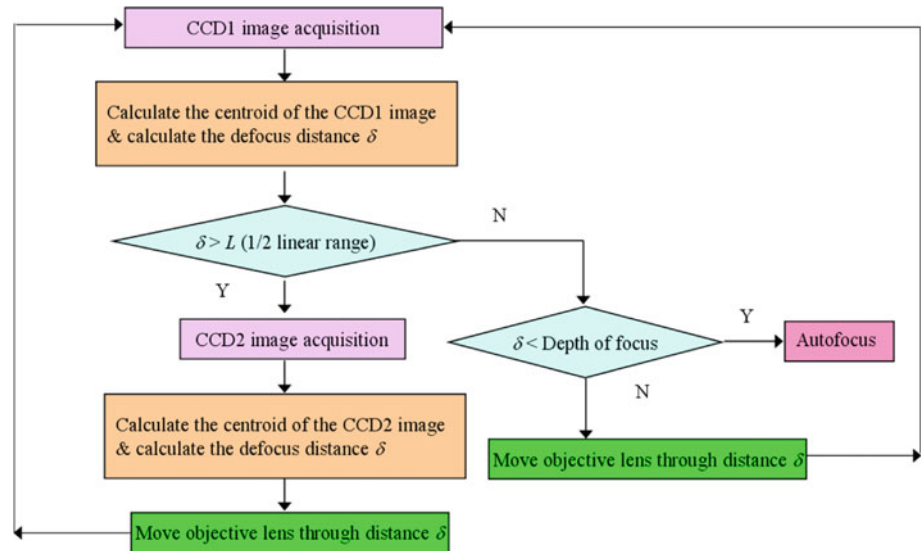


Fig. 7 Output and motion characteristics of proposed autofocusing microscope

Fig. 8 Flow chart of autofocus-processing algorithm in proposed optics-based autofocusing microscope



words, of the two autofocusing methods presented in Figs. 5 and 7, respectively, the proposed autofocusing microscope has a larger linear autofocusing range and a more rapid response, but maintains an equivalent focusing accuracy.

3.3 Numerical characterization of proposed autofocusing microscope

A series of ray-tracing simulations were performed to verify the focusing performance of the proposed autofocusing microscope and to determine suitable values of the major design parameters (i.e., d , f_1 , f_2 , K , and so on).

Figure 9a, b illustrates the detailed structure of the proposed autofocusing microscope and the optical model constructed using commercial ZEMAX software. Table 1 summarizes the selected values of each design parameter.

Figure 10 presents the simulation results obtained for the laser spot shapes on CCD1 and CCD2, respectively, given different values of the defocus position. Meanwhile, Fig. 11 illustrates the simulation results obtained for the variation of the image centroid with the defocus distance in the two optical paths. Figures 10 and 11 show that a linear relationship exists between the centroid coordinates ($x_{centroid}$, $y_{centroid}$) of the detected image and the defocus distance δ . In other words, the numerical results are consistent

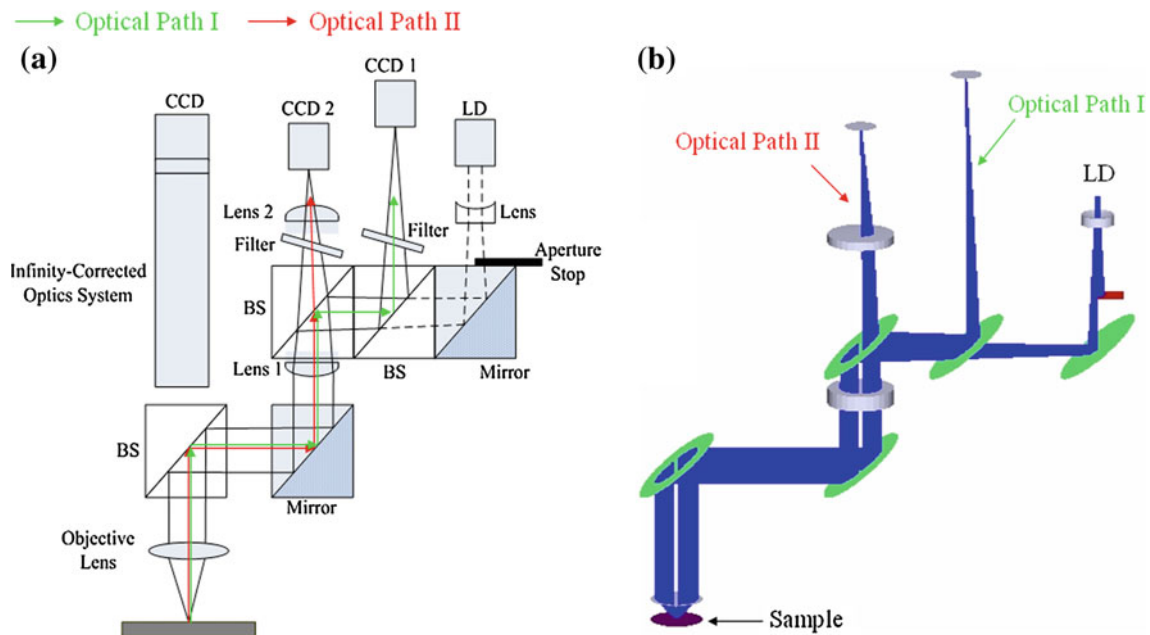


Fig. 9 a Detailed structure of proposed autofocusing microscope, b ZEMAX optical model of proposed autofocusing microscope

Table 1 Design parameters of proposed autofocusing microscope

Variable	Optical Path I	Optical Path II
Focal length of objective lens f_1 (mm)	10	10
Focal length of lens 1 (mm)	200	200
Focal length of lens 2 (mm)	–	100
Distance between lens 1 and lens 2 (mm)	–	52
Equivalent focal length of achromatic lens f_2 (mm)	200	90.74
K	20	9.074
K_I/K_{II}	2.2	

with the theoretical analysis presented in Sect. 3.1. The relationship between the image centroid coordinates $(x_{centroid}, y_{centroid})$ and the defocus distance δ in Optical Path I and Optical Path II is given as follows:

$$\text{centroid } (x_{centroid}, y_{centroid}) = -6.93\delta, \tag{13I}$$

$$\text{centroid } (x_{centroid}, y_{centroid}) = -3.18\delta. \tag{13II}$$

(Note that Eqs. (13I) and (13II) were obtained via a linear curve fitting technique performed using Microsoft Office Excel.) It is noted that the ratio of the slope of the linear curve in Eq. (13I) to that of the linear curve in Eq. (13II) is equal to 2.18 (= 6.93/3.18).

4 Experimental characterization of prototype autofocusing microscope

The validity of the proposed autofocusing microscope was verified by constructing a laboratory-built prototype equipped with a human machine interface (HMI) written in LabVIEW. Figure 12 presents two photographs of the laboratory-built prototype, while Fig. 13 shows experimental images of the laser spot on the two CCD sensors given different values of the defocus distance. Finally, Fig. 14 illustrates the

Fig. 10 Simulation results for shape of laser spot on CCD sensor given different values of the defocus distance

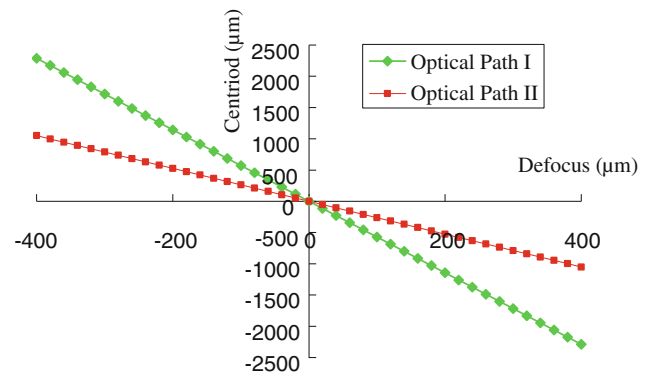
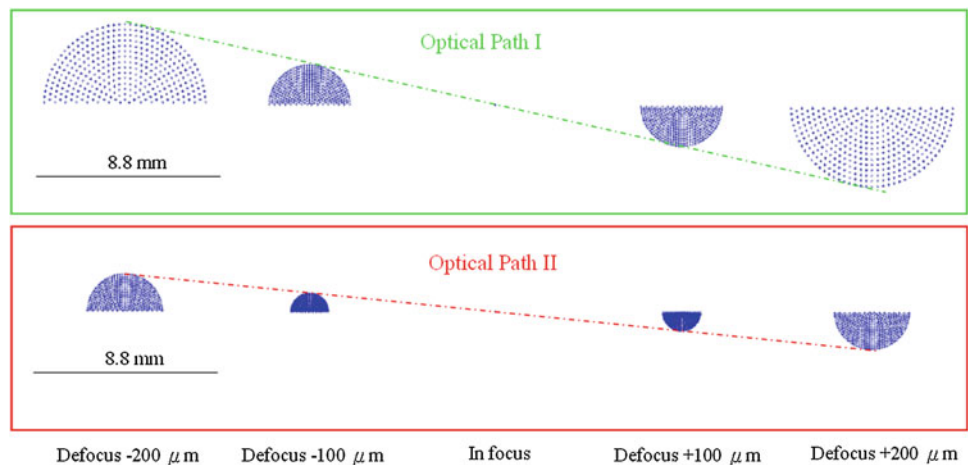


Fig. 11 Simulation results for variation of image centroid position with defocus distance

variation of the image centroid position with the defocus distance in the two optical paths. Figures 13 and 14 show that in both optical paths, the image centroid position varies linearly with the defocus distance δ over a certain defocus range. In other words, the experimental results are consistent with the theoretical results presented in Sect. 3.3. In Fig. 14, the linear relationships between the image centroid coordinates $(x_{centroid}, y_{centroid})$ and the defocus distance δ in Optical Path I and Optical Path II are given, respectively, by

$$\text{centroid } (x_{centroid}, y_{centroid}) = -6.99\delta, \tag{14I}$$

$$\text{centroid } (x_{centroid}, y_{centroid}) = -3.26\delta. \tag{14II}$$

(Note that Eqs. (14I) and (14II) were obtained by applying a linear curve fitting technique to the experimental results presented in Fig. 14 using Microsoft Office Excel.) The ratio of the slope of the linear curve in Eq. (14I) to that of the linear curve in Eq. (14II) is 2.14 (= 6.99/3.26). It is noted that this experimental value is in good agreement with the theoretical value of 2.18 given in Sect. 3.3.

However, in Optical Path I of Fig. 14, it is interesting to note that a nonlinear autofocusing range exists outside the linear autofocusing range. This is because when the

Fig. 12 **a** Photograph of laboratory-built prototype, **b** magnified view of region A in (a)

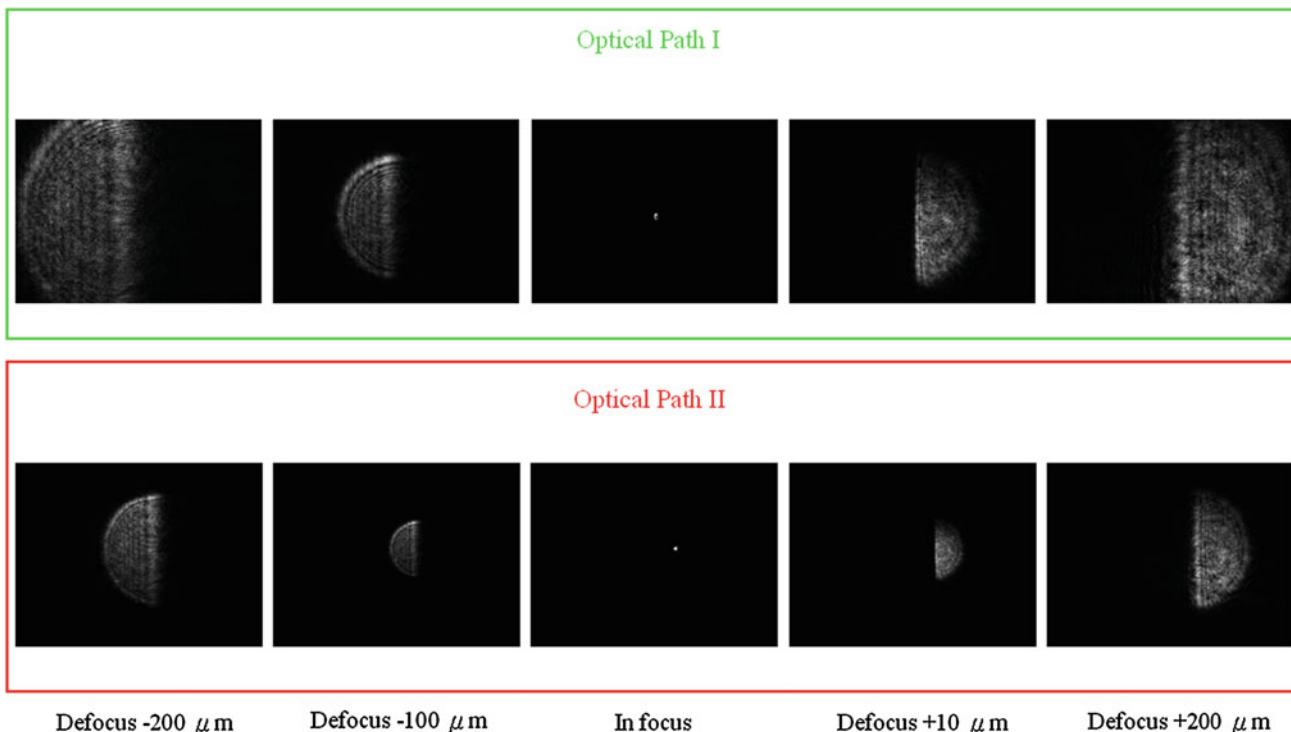
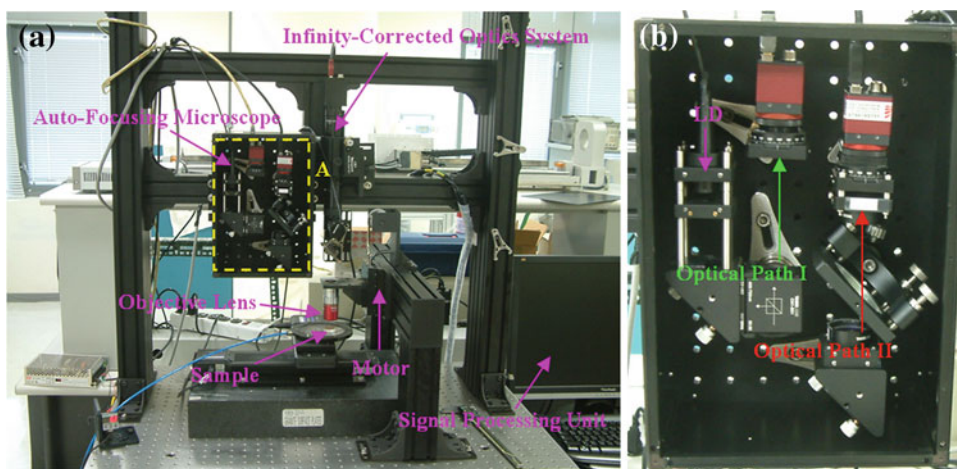


Fig. 13 Experimental results for shape of laser spot on CCD sensors given different values of the defocus distance

defocus distance δ is located outside of this linear range, the reflected laser beam grows bigger, and a certain part of the reflected laser beam is incident on the region outside the CCD chip of CCD1, as shown in Fig. 13. As a result, CCD1 can not capture the total intensity of the reflected laser beam, and the centroid of the image captured by CCD1 has a nonlinear situation.

To demonstrate the feasibility of the proposed auto-focusing microscope, an auto-focusing experiment was conducted using a mirror sample and an initial defocus distance of $\delta = 400 \mu\text{m}$. For comparison purposes, the experiment was also performed using the conventional auto-focusing structure with centroid method shown in

Fig. 3. The experimental results obtained using the conventional and proposed auto-focusing microscopes are shown in the video sequences presented in Figs. 15 and 16, respectively. In Fig. 15, it is seen that in the conventional auto-focusing microscope with centroid method, the objective lens is moved from the initial defocus distance of $400 \mu\text{m}$ to a distance of $153.2 \mu\text{m}$ and is then moved through two further displacements to the final focusing position (yielding a focusing accuracy of less than $2 \mu\text{m}$). By contrast, Fig. 16 shows that in the proposed auto-focusing microscope, the objective lens is moved from the initial defocus position of $400 \mu\text{m}$ to a new position of $31 \mu\text{m}$ and is then moved directly to the final focusing

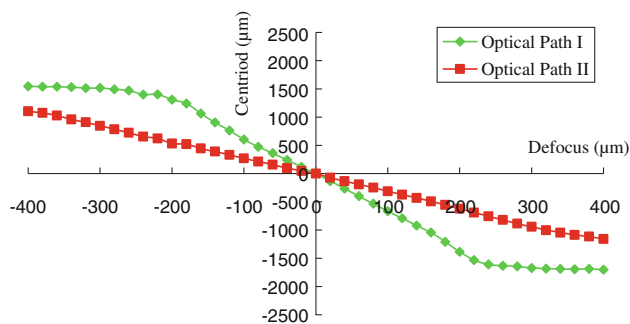


Fig. 14 Experimental results for variation of image centroid position with defocus distance

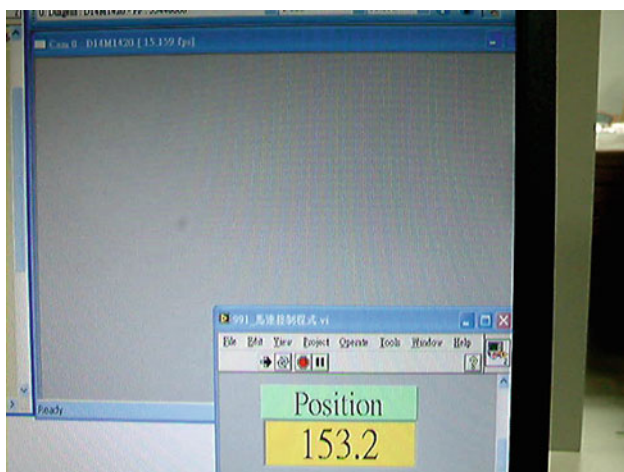


Fig. 15 Dynamic testing video of conventional autofocus microscope with centroid method and mirror sample



Fig. 16 Dynamic testing video of proposed autofocus microscope with mirror sample

position (again, with a focusing accuracy of less than $2\ \mu\text{m}$). Note that the objective lens can be moved directly via a linear motor (piezo-electric motor, HR8 series,

Nanomotion Inc.) featuring a closed-loop control scheme based upon a feedback signal generated with an optical encoder (resolution of $0.1\ \mu\text{m}$). Therefore, the final focusing position was measured by using a position feedback signal from the optical encoder. In other words, compared to the conventional method with centroid method, the proposed autofocus microscope yields an equivalent focusing accuracy, but has both a larger linear autofocusing range and a more rapid response.

5 Conclusions

This study has presented a novel optics-based autofocus microscope with both a large linear autofocusing range and a rapid response. The proposed microscope comprises two optical paths. Optical Path I achieves a precise focusing accuracy over a short linear autofocusing range, while Optical Path II achieves a lower focusing accuracy, but over a longer linear autofocusing range. The two optical paths are combined using a self-written autofocus-processing algorithm to achieve a rapid autofocusing capability over a large linear autofocusing range without any loss in the focusing accuracy. The performance of the proposed microscope has been demonstrated using a laboratory-built prototype. The experimental results have shown that the proposed microscope has a larger linear autofocusing range and a faster response time than a conventional autofocus microscope with centroid method, but achieves a comparable focusing performance (less than $2\ \mu\text{m}$). As a result, the proposed microscope provides an ideal solution for a wide range of optical inspection and industrial applications.

Acknowledgments The authors gratefully acknowledge the financial support provided to this study by the National Science Council of Taiwan under Grant No. NSC 100-2218-E-194-008. The authors would like to express their thanks to Mr. Yu-Hsiu Chang of the Laser Application Technology Center, Industrial Technology Research Institute, Taiwan, for his technological assistance throughout the course of the study.

References

1. J.H. Kang, C.B. Lee, J.Y. Joo, S.K. Lee, Phase-locked loop based on machine surface topography measurement using lensed fibers. *Appl. Opt.* **50**, 460–467 (2011)
2. P. Petruck, R. Riesenberger, R. Kowarschik, Optimized coherence parameters for high resolution holographic microscopy. *Appl. Phys. B* **106**, 339–348 (2012)
3. Z. Zhang, Q. Feng, Z. Gao, C. Kuang, C. Fei, Z. Li, J. Ding, A new laser displacement sensor based on triangulation for gauge real-time measurement. *Opt. Laser Technol.* **40**, 252–255 (2008)
4. W.Y. Hsu, C.S. Lee, P.J. Chen, N.T. Chen, F.Z. Chen, Z.R. Yu, C.H. Kuo, C.H. Hwang, Development of the fast astigmatic auto-focus microscope system. *Meas. Sci. Technol.* **20**, 045902-1–045902-9 (2009)

5. S.B. Andersson, A nonlinear controller for three-dimensional tracking of a fluorescent particle in a confocal microscope. *Appl. Phys. B* **104**, 161–173 (2011)
6. J.G. Ritter, R. Veith, J.P. Siebrasse, U. Kubitscheck, High-contrast single-particle tracking by selective focal plane illumination microscopy. *Opt. Express* **16**, 7142–7152 (2008)
7. P. Calzavara-Pinton, C. Longo, M. Venturini, R. Sala, G. Pellacani, Reflectance confocal microscopy for in vivo skin imaging. *Photochem. Photobiol.* **84**, 1421–1430 (2008)
8. M. Zeder, J. Pernthaler, Multispot live-image autofocusing for high-throughput microscopy of fluorescently stained bacteria. *Cytom. Part A* **75A**, 781–788 (2009)
9. T. Pengo, A. Munoz-Barrutia, C. Ortiz-De-Solorzano, Halton sampling for autofocus. *J. Microsc.* **235**, 50–58 (2009)
10. H.C. Chang, T.M. Shih, N.Z. Chen, N.W. Pu, A microscope system based on bevelaxial method auto-focus. *Opt. Lasers Eng.* **47**, 547–551 (2009)
11. C.Y. Chen, R.C. Hwang, Y.J. Chen, A passive auto-focus camera control system. *Appl. Soft Comput.* **10**, 296–303 (2010)
12. M.A. Bueno-Ibarra, J. Alvarez-Borrego, L. Acho, M.C. Chavez-Sanchez, Fast autofocus algorithm for automated microscopes. *Opt. Eng.* **44**, 063601-1–063601-8 (2005)
13. V.V. Bezzubik, S.N. Ustinov, N.R. Belashenkov, Optimization of algorithms for autofocusing a digital microscope. *J. Opt. Technol.* **76**(10), 603–608 (2009)
14. Y. Liron, Y. Paran, N.G. Zatorsky, B. Geiger, Z. Kam, Laser autofocusing system for high-resolution cell biological imaging. *J. Microsc.* **221**, 145–151 (2006)
15. J.H. Lee, Y.S. Kim, S.R. Kim, I.H. Lee, H.J. Pakh, Real-time application of critical dimension measurement of TFT-LCD pattern using a newly proposed 2D image-processing algorithm. *Opt. Lasers Eng.* **46**, 558–569 (2008)
16. S.L. Brazdilova, M. Kozubek, Information content analysis in automated microscopy imaging using an adaptive autofocus algorithm for multimodal functions. *J. Microsc.* **236**, 194–202 (2009)
17. S. Yazdanfar, K.B. Kenny, K. Tasimi, A.D. Corwin, E.L. Dixon, R.J. Filkins, Simple and robust image-based autofocusing for digital microscopy. *Opt. Express* **16**, 8670–8677 (2008)
18. C.H. Chen, T.L. Feng, Fast 3D shape recovery of a rough mechanical component from real time passive autofocus system. *Int. J. Adv. Manuf. Technol.* **34**, 944–957 (2007)
19. E.F. Wright, D.M. Wells, A.P. French, C. Howells, N.M. Everitt, A low-cost automated focusing system for time-lapse microscopy. *Meas. Sci. Technol.* **20**, 027003-1–027003-4 (2009)
20. H. Oku, M. Ishikawa, High-speed autofocusing of a cell using diffraction patterns. *Opt. Express* **14**, 3952–3960 (2006)
21. P. Langehanenberg, B. Kemper, D. Dirksen, G. von Bally, Autofocusing in digital holographic phase contrast microscopy on pure phase objects for live cell imaging. *Appl. Opt.* **47**, D176–D182 (2008)
22. T. Kim, T.C. Poon, Autofocusing in optical scanning holography. *Appl. Opt.* **48**, H153–H159 (2009)
23. S. Lee, J.Y. Lee, W. Yang, D.Y. Kim, Autofocusing and edge detection schemes in cell volume measurements with quantitative phase microscopy. *Opt. Express* **17**, 6476–6486 (2009)
24. M. Moscaritolo, H. Jampel, F. Knezevich, R. Zeimer, An image based auto-focusing algorithm for digital fundus photography. *IEEE Trans. Med. Imaging* **28**, 1703–1707 (2009)
25. Y. Shao, J. Qu, H. Li, Y. Wang, J. Qi, G. Xu, H. Niu, High-speed spectrally resolved multifocal multiphoton microscopy. *Appl. Phys. B* **99**, 633–637 (2010)
26. S.J. Abdullah, M.M. Ratnam, Z. Samad, Error-based autofocus system using image feedback in a liquid-filled diaphragm lens. *Opt. Eng.* **48**, 123602-1–123602-9 (2009)
27. R.M. Wasserman, P.G. Gladnick, K.W. Atherton, Systems and methods for rapidly automatically focusing a machine vision inspection system, U.S. Patent 7030351B2 (2006)
28. J.Y. Lee, Y.H. Wang, L.J. Lai, Y.J. Lin, Y.H. Chang, Development of an auto-focus system based on the Moiré method. *Measurement* **44**, 1793–1800 (2011)
29. I. Chremmos, N.K. Efremidis, D.N. Christodoulides, Pre-engineered abruptly autofocusing beams. *Opt. Lett.* **36**, 1890–1892 (2011)
30. B.J. Jung, H.J. Kong, B.G. Jeon, D.Y. Yang, Y. Son, K.S. Lee, Autofocusing method using fluorescence detection for precise two-photon nanofabrication. *Opt. Express* **19**, 22659–22668 (2011)
31. P. Zhang, J. Prakash, Z. Zhang, M.S. Mills, N.K. Efremidis, D.N. Christodoulides, Z. Chen, Trapping and guiding microparticles with morphing autofocusing Airy beams. *Opt. Lett.* **36**, 2883–2885 (2011)
32. D.K. Cohen, W.H. Gee, M. Ludeke, J. Lewkowicz, Automatic focus control: the astigmatic lens approach. *Appl. Opt.* **23**, 565–570 (1984)
33. K.C. Fan, C.L. Chu, J.I. Mou, Development of a low-cost autofocusing probe for profile measurement. *Meas. Sci. Technol.* **12**, 2137–2146 (2001)
34. Q.P. Li, F. Ding, P. Fang, Flash CCD laser displacement sensor. *Electron. Lett.* **42**, 910–912 (2006)
35. Y. Tanaka, T. Watanabe, K. Hamamoto, H. Kinoshita, Development of nanometer resolution focus detector in vacuum for extreme ultraviolet microscope. *Jpn. J. Appl. Phys.* **45**, 7163–7166 (2006)
36. S.J. Lee, D.Y. Chang, A laser sensor with multiple detectors for freeform surface digitization. *Int. J. Adv. Manuf. Technol.* **31**, 1181–1190 (2007)
37. Z. Li, K. Wu, Autofocus system for space cameras. *Opt. Eng.* **44**, 053001-1–053001-5 (2005)
38. H.G. Rhee, D.I. Kim, Y.W. Lee, Realization and performance evaluation of high speed autofocusing for direct laser lithography. *Rev. Sci. Instrum.* **80**, 073103-1–073103-5 (2009)
39. Y. Nishio, Optical displacement meter, optical displacement measuring method, optical displacement measuring program, computer-readable recording medium, and device that records the program, U.S. Patent 7489410B2 (2009)
40. M. Kataoka, K. Nemoto, Focusing servo device and focusing servo method, U.S. Patent 7187630B2 (2007)
41. M. He, W. Zhang, X. Zhang, A displacement sensor of dual-light based on FPGA. *Optoelectron. Lett.* **3**, 294–298 (2007)
42. K.H. Kim, S.Y. Lee, S. Kim, S.G. Jeong, DNA microarray scanner with a DVD pick-up head. *Curr. Appl. Phys.* **8**, 687–691 (2008)
43. S.H. Wang, C.J. Tay, C. Quan, H.M. Shang, Z.F. Zhou, Laser integrated measurement of surface roughness and micro-displacement. *Meas. Sci. Technol.* **11**, 454–458 (2000)
44. A. Weiss, A. Obotnine, A. Lasinski, Method and apparatus for the auto-focussing infinity corrected microscopes, U.S. Patent 7700903 (2010)